A CANDIDATE DUAL ACTIVE GALACTIC NUCLEUS AT $z = 1.175$

R. Scott Barrows[1], Daniel Stern[2], Kristin Madsen[3], Fiona Harrison[3], Roberto J. Assef[2], Julia M. Comerford[4],
Michael C. Cushing[2], Christopher D. Fassnacht[5], Anthony H. Gonzalez[6], Roger Griffith[7], Ryan Hickox[8],
J. Davy Kirkpatrick[7], and David J. Lagattuta[5]

[1] Arkansas Center for Space and Planetary Sciences, University of Arkansas, Fayetteville, AR 72701, USA; rbarrows@uark.edu
[2] Jet Propulsion Laboratory, California Institute of Technology, 4800 Oak Grove Drive, Pasadena, CA 91109, USA
[3] California Institute of Technology, 1200 East California Boulevard, Pasadena, CA 91125, USA
[4] Astronomy Department, University of Texas at Austin, Austin, TX 78712, USA
[5] Department of Physics, University of California at Davis, One Shields Avenue, Davis, CA 95616, USA
[6] Department of Astronomy, University of Florida, Gainesville, FL 32611, USA
[7] Infrared Processing and Analysis Center, California Institute of Technology, Pasadena, CA 91125, USA
[8] Department of Physics, Durham University, Durham DHI 3LE, UK

ABSTRACT

The X-ray source CXOXBJ142607.6+353351 (CXOJ1426+35), which was identified in a 172 ks *Chandra* image in the Boötes field, shows double-peaked rest-frame optical/UV emission lines, separated by 0″.69 (5.5 kpc) in the spatial dimension and by 690 km s^{-1} in the velocity dimension. The high excitation lines and emission line ratios indicate both systems are ionized by an active galactic nucleus (AGN) continuum, and the double-peaked profile resembles that of candidate dual AGNs. At a redshift of $z = 1.175$, this source is the highest redshift candidate dual AGN yet identified. However, many sources have similar emission line profiles for which other interpretations are favored. We have analyzed the substantial archival data available in this field as well as acquired near-infrared (NIR) adaptive optics (AO) imaging and NIR slit spectroscopy. The X-ray spectrum is hard, implying a column density of several 10^{23} cm^{-2}. Though heavily obscured, the source is also one of the brightest in the field, with an absorption-corrected 2–10 keV luminosity of $\sim 10^{45}$ erg s^{-1}. Outflows driven by an accretion disk may produce the double-peaked lines if the central engine accretes near the Eddington limit. However, we may be seeing the narrow line regions of two AGNs following a galactic merger. While the AO image reveals only a single source, a second AGN would easily be obscured by the significant extinction inferred from the X-ray data. Understanding the physical processes producing the complex emission line profiles seen in CXOJ1426+35 and related sources is important for interpreting the growing population of dual AGN candidates.

Key words: galaxies: active – galaxies: individual (CXOXBJ142607.6+353351) – galaxies: nuclei – quasars: emission lines

Online-only material: color figure

1. INTRODUCTION

It is now generally believed that galaxies evolve in a hierarchical fashion with galaxies growing through mergers. Furthermore, evidence suggests that most, if not all, galaxies contain a supermassive black hole (SMBH) at their center (Richstone et al. 1998). Therefore, in a galactic merger the force of dynamical friction will act to bring each SMBH toward the center of the new mass distribution, first forming a dual SMBH (separations of several kpc), then a gravitationally bound system (subparsec separations) and eventually merging to form a single, more massive SMBH. The amount of time spent in each stage is dependent upon the efficiency of the processes carrying away angular momentum from the system (Begelman et al. 1980). At large separations (>10–100 pc), the primary force acting on the SMBHs is dynamical friction from the surrounding gas and dust. As the SMBHs form a binary system (i.e., harden), ejection of stars becomes most important. Finally at close separations ($<10^{-2}$ pc), gravitational radiation will become the most important mechanism of energy loss (Milosavljević & Merritt 2003).

Numerical simulations show that in a wet merger (i.e., where the merging galaxies possess a significant fraction of gas and dust), tidal interactions are effective at funneling the gas and dust toward the center of the merging system where the two

SMBHs are located, providing fuel for enhanced accretion (Hernquist 1989). This process is thought to be a possible mechanism for initiating an active galactic nucleus (AGN) or quasar phase (Hopkins et al. 2005, 2008), and the existence of a dual AGN (two actively accreting SMBHs within the same galaxy) is a natural prediction of this merger fueling model. Therefore, identifying pairs of SMBHs in the process of merging is extremely important for probing the link between AGN activity and galaxy evolution.

Unfortunately, observational evidence of such systems has proven very difficult to obtain. Large samples of binary quasars exist as evidence for quasar clustering and mutual triggering (Hennawi et al. 2006, 2010; Myers et al. 2007, 2008; Foreman et al. 2009). However, these are typically at large projected separations (>10 kpc) and thus generally only represent the earliest stage of binary SMBH evolution. Most confirmed cases of dual SMBHs at smaller separations (between 10 kpc and 1 kpc) have been identified in local ultraluminous infrared galaxies (ULIRGs) as pairs of X-ray point sources (Komossa et al. 2003; Guainazzi et al. 2005; Hudson et al. 2006; Bianchi et al. 2008; Piconcelli et al. 2010; Koss et al. 2011), with much of the optical emission obscured by the heavy internal extinction common in ULIRGs. In some cases the obscuration is so heavy that only one nucleus is visible, thus highlighting the difficulty that dusty, merging systems present to identification

of dual AGNs. Additionally, the close (7 pc separation) binary SMBH system in the radio galaxy 0402+379 was identified from Very Long Baseline Array (VLBA) observations (Rodriguez et al. 2006). While the excellent spatial resolution achievable in the radio regime makes the VLBA capable of detecting close binaries, this technique is time consuming and not suited to identifying a large sample of sources.

In the past few years, several interesting individual examples of dual/binary SMBH candidates have been identified from single-epoch optical spectra of AGNs or quasars showing double-peaked emission lines. The Sloan Digital Sky Survey (SDSS) spectral archive (Abazajian et al. 2009) has been a fruitful database for such identifications. However, these objects do not represent a homogeneous class, and thus the physical interpretation of many of them, based on single-epoch fiber spectra alone, remains ambiguous.

For example, the sources SDSS J153636.22+044127.0 (J1536+0441, Boroson & Lauer 2009) and SDSS J105041.35+ 345631.3 (J1050+3456, Shields et al. 2009b) show double-peaked, broad Balmer emission lines (Hα, Hβ, and Hγ), which resemble two broad-line regions (BLRs) with significant velocity differences (>2000 km s^{-1}). However, these objects might instead be members of the sub-class of AGNs/quasars called "double-peaked emitters" (also known as "disk emitters") where the double peaks of the Balmer lines are attributed to emission from a single accretion disk. Line emission contribution from an accretion disk is suggested by the extended wings in the Balmer emission lines (particularly evident in Hα, e.g., Chornock et al. 2010) which is a characteristic disk profile feature. On the other hand, these sources are extreme examples of "disk emitters," and it has been shown that such strongly double-peaked Balmer lines in quasars may represent cases in which the presence of a secondary SMBH is effective at enhancing the double-peaked profile produced by the disk (Tang & Grindlay 2009; Barrows et al. 2011). One such object, 4C+22.25, identified by Decarli et al. (2010) as a candidate binary SMBH, shows very high (8700 km s^{-1}) velocity offsets between the two peaks of the Balmer emission lines; it is therefore unlikely to be a "disk emitter" as the velocity difference is several thousand km s^{-1} larger than that of any known similar source (see the sample of Strateva et al. 2003). These results demonstrate the diversity of double-peaked broad line profiles and emphasize that in a close binary SMBH there are likely to be strong interactions between the SMBHs and the accretion disks.

A growing number of objects have been identified with narrow forbidden emission lines that are either offset from the systemic velocity or double-peaked in single-epoch spectra, many of which have been found through systematic searches for candidate dual AGNs, both in the DEEP2 Galaxy Redshift Survey (Comerford et al. 2009b) and SDSS (Zhou et al. 2004; Wang et al. 2009; Smith et al. 2010; Liu et al. 2010b). Specifically, objects have been identified as dual AGN candidates because they show strongly double-peaked [O III]5007 lines (Zhou et al. 2004; Gerke et al. 2007; Peng et al. 2011), or double peaks in all of the narrow lines, both permitted and forbidden, e.g., SDSS 092712.65+294344.0 (J0927+2943, Komossa et al. 2008b; Bogdanović et al. 2009b; Dotti et al. 2009). These double peaks indicate two sets of narrow emission line regions (NLRs) and are suggestive of dual AGNs with separations up to several kpc. These systems are excellent sources for study because, at the implied kpc-scale separations, the two putative AGNs can be resolved in two-dimensional spectroscopy and imaging.

However, double-peaked narrow lines have been seen in a number of AGNs and quasars where other physical explanations have been favored. For example, NLRs are thought to have complex gas kinematics which may include radially flowing material capable of producing offset or double-peaked narrow emission lines (Heckman et al. 1981). In particular, powerful radio galaxies often show complex, spatially extended NLRs with multiple components aligned along the radio axis (see reviews of radio galaxies in McCarthy 1993 and Miley & De Breuck 2008). Models for this alignment include reflection of the AGN emission (Tadhunter et al. 1988), jet-induced star formation (De Young 1981), inverse Compton scattering of cosmic microwave background photons off the relativistic electrons in the radio jet (Daly 1992), material out-flowing from an accretion disk or entrained in a radio jet (Holt et al. 2003, 2008; Komossa et al. 2008a), as well as a combination of shocks and photoionization by the central engine (Maxfield et al. 2002). There is an extensive literature on the spatially extended, kinematically complex NLRs of powerful radio galaxies (van Ojik et al. 1996; Villar-Martín et al. 2000, 2007, 2010; Zirm et al. 2005; Nesvadba et al. 2006). Though radio galaxy NLRs often appear vaguely reminiscent of dual AGN candidates, multiple AGNs are rarely suggested as possible interpretations of the complex radio galaxy NLRs. Finally, simple geometrical interpretations have been invoked to explain double-peaked narrow lines in AGNs, such as a rotating, disk-shaped NLR or a single AGN illuminating two NLRs (Xu & Komossa 2009).

Developing a clear understanding of the physical process producing these often complex emission line profiles is important to both the search for dual AGNs and to further understand quasar/AGN emission line regions in general. Since it is clear that a number of physical processes other than a pair of AGNs can explain double-peaked emission lines (broad and/or narrow), more information is necessary to entirely reject or confirm any one model. From single-epoch spectra, emission line ratios may be used as diagnostic tools to constrain the nature of the ionizing continuum producing each set of emission lines. Other observational tools include spatially resolved spectroscopy, synoptic spectroscopic observations, and high-resolution imaging.

In this paper, we discuss the X-ray source CXOXBJ142607.6+353351 (from here on CXOJ1426+35) which was originally identified as an X-ray source in the Boötes field (Wang et al. 2004). In follow-up slit spectroscopy, CXOJ1426+35 showed double rest-frame optical/UV emission lines, separated spatially by 0″.69, and in velocity space by 690 km s^{-1}, as measured from the [O III]5007 line. We discuss CXOJ1426+35 as an example of a candidate dual AGN and place its spectral and morphological properties within the context of other candidate dual/binary SMBHs. We examine a variety of possible explanations for the double-peaked emission lines. Interestingly, CXOJ1426+35 is at $z = 1.175$, the highest redshift yet for a candidate dual AGN, where previously candidates were identified out to $z \approx 0.8$. At this redshift, we have access to rest-frame UV emission lines which are unique among the current sample of candidate dual AGNs in the literature. Section 2 discusses the known properties of CXOJ1426+35 and Section 3 discusses various physical interpretations of the data. Section 4 takes CXOJ1426+35 as a pedagogical example to describe a number of methods by which candidate dual/binary SMBHs may be confirmed or rejected. Section 5 contains the conclusions. Throughout the paper we assume cosmological parameters of $H_0 = 70$ km s^{-1} kpc^{-1}, $\Omega_M = 0.30$, and $\Omega_\Lambda = 0.70$.

Table 1
Photometric Data for CXOJ1426+35

Obs. Bandpass	Rest Bandpass	m_{AB}	m_{Vega}	F_ν (μJy)[e]	Detector/Instrument
2–10 keV	13.0 keV	. . .	. . .	$2.81^{+0.33}_{-0.30} \times 10^{-3}$	*Chandra*/ACIS
0.5–2 keV	2.7 keV	. . .	. . .	$4.44^{+4.01}_{-2.11} \times 10^{-5}$	*Chandra*/ACIS
2271 Å[a]	1060 Å	22.24 ± 0.02	20.57 ± 0.02	$4.63^{0.10}_{0.09}$	*GALEX*/NUV
u[b]	1630 Å	21.56 ± 0.23	20.56 ± 0.23	$8.95^{+2.01}_{-1.64}$	SDSS
g[b]	2190 Å	21.78 ± 0.09	21.87 ± 0.09	$7.05^{+0.54}_{-0.50}$	SDSS
r[b]	2865 Å	21.26 ± 0.09	21.10 ± 0.09	$11.38^{+0.87}_{-0.81}$	SDSS
i[b]	3505 Å	20.71 ± 0.09	20.32 ± 0.09	$18.88^{+1.44}_{-1.34}$	SDSS
z[b]	4200 Å	20.50 ± 0.26	19.98 ± 0.26	$22.49^{+6.09}_{-4.79}$	SDSS
J[c]	5975 Å	20.37 ± 0.09	19.46 ± 0.09	$26.16^{+2.72}_{-2.47}$	NOAO/NEWFIRM
H[c]	7585 Å	20.41 ± 0.28	19.02 ± 0.28	$25.34^{+8.13}_{-6.17}$	NOAO/NEWFIRM
K_s[c]	1.0 μm	20.10 ± 0.58	18.25 ± 0.58	$33.53^{+24.69}_{-14.23}$	NOAO/NEWFIRM
3.6 μm[d]	1.7 μm	19.76 ± 0.02	16.97 ± 0.02	$45.77^{+1.53}_{-1.49}$	*Spitzer*/IRAC
4.5 μm[d]	2.1 μm	19.47 ± 0.02	16.21 ± 0.02	$58.96^{+1.97}_{-1.91}$	*Spitzer*/IRAC
5.8 μm[d]	2.7 μm	18.87 ± 0.06	15.14 ± 0.06	$101.09^{+7.32}_{-6.85}$	*Spitzer*/IRAC
8.0 μm[d]	3.7 μm	17.97 ± 0.03	13.57 ± 0.03	$242.24^{+10.24}_{-9.87}$	*Spitzer*/IRAC

Notes.
[a] Magnitude determined for the 3″.8 radius aperture corrected to total magnitude (see Section 2.1.2).
[b] SDSS model magnitudes (see Section 2.1.3).
[c] Magnitudes are for a Kron-like elliptical aperture (see Section 2.1.3).
[d] Magnitudes determined for the 4″ radius aperture corrected to total magnitudes (see Section 2.1.4).
[e] The *Chandra* flux densities are not absorption-corrected.

2. PROPERTIES OF THE SOURCE

In an attempt to understand the nature of the complex line emission of CXOJ1426+35, we first summarize in this section the known properties of the source. The multi-wavelength data available for CXOJ1426+35 include both archival data and newly obtained data from the Keck II telescope in Hawaii.

2.1. Archival Data

The photometric properties of CXOJ1426+35 from archival observations are summarized in Table 1. The mid-IR through near-ultraviolet (NUV) colors are displayed as a broadband spectral energy distribution (SED) with best-fitting spectral templates in Section 2.3. We begin by describing the archival observations.

2.1.1. Chandra X-Ray Data

CXOJ1426+35 was detected with the Advanced CCD Imaging Spectrometer (ACIS-I; Garmire et al. 2003) on board *Chandra* in a 172 ks image of the Large Area Lyman Alpha Boötes field (Wang et al. 2004). The total image was composed of two exposures taken on 2002 April 16–17 and June 9. In Wang et al. (2004), the reported number of background-subtracted soft (0.5–2.0 keV) and hard (2.0–7.0 keV) counts, determined by "wavdetect," are $24.3^{+6.6}_{-5.4}$ and $240.8^{+17.2}_{-11.0}$, respectively, which yields a hardness ratio (defined as HR $\equiv (H - S)/(H + S)$, where H and S are the number of the hard and soft counts, respectively) of 0.82. Assuming Galactic absorption and a power-law spectrum, the hardness ratio corresponds to a photon index of $\Gamma = -1.3$, which is significantly harder than the typical observed $\Gamma = 1.4$ of AGNs when not corrected for absorption. Interestingly, out of 168 sources detected in the field by Wang et al. (2004), only 13 have larger 0.5–10 keV fluxes and only 7 are more obscured (i.e., have higher hardness ra-

tios); no brighter sources have higher hardness ratios. Thus, CXOJ1426+35 is unique in that it is both relatively bright and heavily obscured (i.e., Figure 2 of Wang et al. 2004). Unfortunately, the off-axis detection of CXOJ1426+35 means that it is unresolved by *Chandra*. However, the high number of hard counts allowed us to obtain a reasonable spectrum. To do so, we re-reduced the data using the CIAO software, following the standard procedure for extracting source and background regions, and creating response files for spectral analysis. The two observations were processed independently. In each event file, we extracted a source region 30 pixels (15″) in diameter centered on the centroid position of the source and a background region 50 pixels (25″) in diameter adjacent to the source region. The source regions, background regions, and response files were used in XSPEC to perform spectral modeling. For each event file, the spectra were re-binned so that each bin had at least 15 counts. When fitting the models, the same model was fit to the spectrum from each observation simultaneously to place tighter constraints on the parameters. All bad channels were ignored, and the first channel of each data set (where there are few counts) was also ignored. A simple absorbed power law was fit with the redshift frozen at $z = 1.175$ (see Section 2.2.1 for the redshift determination). The spectrum, with the model overlaid and residuals underneath, is shown in Figure 1. The residuals around $\sim$3 keV are suggestive of rest-frame 6.4 keV Fe Kα emission, though there are too few counts to obtain a good line fit. The best-fit parameters are an intrinsic power-law slope $\Gamma = 1.96^{+1.24}_{-0.57}$ and column density $n_H = 5.90^{+4.94}_{-1.81} \times 10^{23}$ cm^{-2}. This column density implies a highly obscured source. From the best-fit model the observed 2–10 keV flux is $5.44^{+0.65}_{-0.58} \times 10^{-14}$ erg s^{-1} cm^{-2} or $2.81^{+0.33}_{-0.30} \times 10^{-3}$ μJy (Table 1) which corresponds to an absorption-corrected intrinsic luminosity of $L_{2-10\,keV} = 9.7^{+3.0}_{-2.3} \times 10^{44}$ erg s^{-1}. From $L_{2-10\,keV}$, the bolometric correction of Hopkins et al. (2007) yields $L_{BOL} \approx 9 \times 10^{46}$ erg s^{-1}.
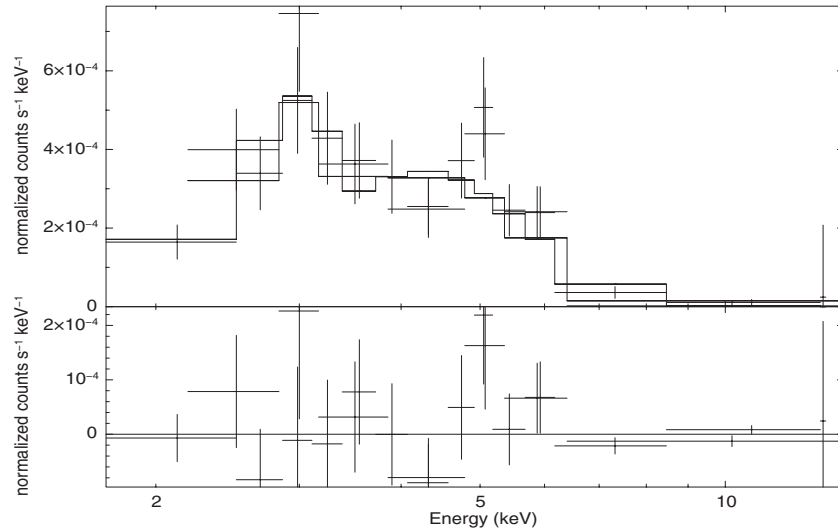
Figure 1. *Chandra*/ACIS spectrum and model residuals of CXOJ1426+35 in the observed frame. The top panel shows the combined data sets of the extractions from both the 120 ks and 58 ks images (in Wang et al. 2004 the 58 ks image was corrected to 52 ks, hence their quoted total time of 172 ks), and the best-fit absorbed power-law model is overlaid. The bottom panel shows the residuals from the best-fit model.

2.1.2. UV Imaging

CXOJ1426+35 was detected by the NUV detector on the *Galaxy Evolution Explorer* (*GALEX*; Martin et al. 2003) which has an observed bandwidth of 1771–2831 Å and effective wavelength of 2271 Å. The 5″ FWHM resolution of the NUV detector on *GALEX* is unable to resolve CXOJ1426+35. Therefore, for photometry we have used the flux measurement from the 3″.8 radius aperture (to most closely match the 4″ radius aperture for the Infrared Array Camera (IRAC) data; Section 2.1.4). We then corrected to a total magnitude using the correction factor from Morrissey et al. (2007) and converted to a Vega magnitude calculated based on the model atmosphere of Vega from Kurucz (1993). The NUV photometry is listed in Table 1. CXOJ1426+35 was not detected by the far-ultraviolet detector on *GALEX*.

2.1.3. Optical/Near-IR Imaging

CXOJ1426+35 is well detected by the SDSS (Figure 2). In Table 1 we list the model magnitudes, calculated by the SDSS pipeline using the best-fitting function (either a deVaucouleurs or an exponential profile—in this case an exponential profile) in the *r* band and applying that model to the other bands. We converted the SDSS magnitudes to AB magnitudes following Bohlin et al. (2001): $AB_{offset} \approx 0.04, 0.0, 0.0, 0.0,$ and -0.02 magnitudes for *u*, *g*, *r*, *i*, and *z*, respectively, where $M_{AB} = M_{SDSS} - AB_{offset}$. We then converted to Vega magnitudes based on the model atmosphere of Vega from Kurucz (1993). Figure 2 shows the stacked *g* + *r* + *i* SDSS image of CXOJ1426+35, revealing a clearly extended host galaxy.

Note that the 8.5 deg² Boötes field has been deeply imaged at optical wavelengths by the NOAO Deep, Wide-Field Survey (NDWFS; Jannuzi et al. 1999). However, the bright star ~25″ east of our target (see Figure 2), while useful for the adaptive optics (AO) observations discussed in Section 2.2.2, severely contaminates the NDWFS photometry for CXOJ1426+35 due to a bright diffraction spike.

The Boötes field has also been deeply imaged at NIR wavelengths (*J*, *H*, and K_s) using the NOAO Extremely Wide-Field Infrared Imager (NEWFIRM; Probst et al. 2004, 2008) on the 4 m Mayall Telescope at Kitt Peak National Observatory. Those data were obtained as part of the Infrared Boötes Imaging
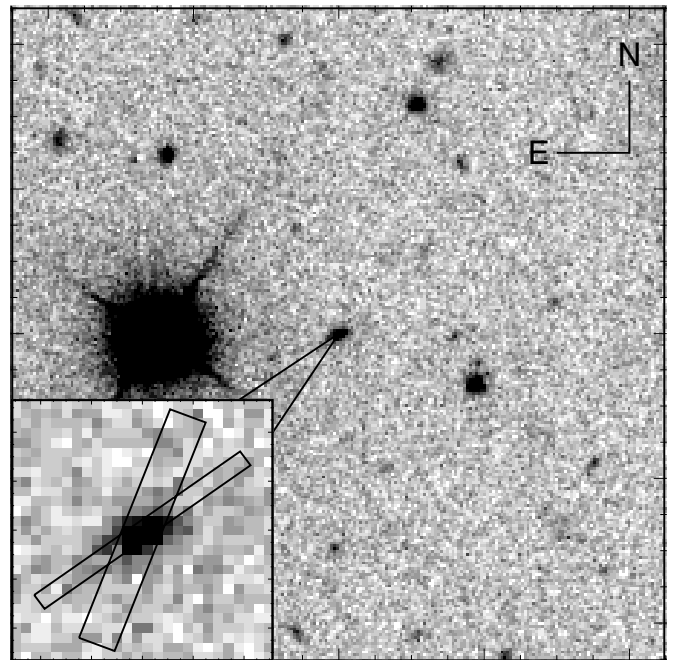

Figure 2. Stacked *g* + *r* + *i* SDSS image centered on the position of CXOJ1426+35. The larger image is 90″ on a side with north up and east to the left. The inset is a close-up of CXOJ1426+35, 10″ on a side, showing that the galaxy is clearly extended with a position angle of P.A. = −54°.1. Boxes show the spectroscopic slit configurations obtained using LRIS (P.A. = −21°, slit width = 1″.5) and NIRSPEC (P.A. = −54°.1, slit width = 0″.7). Note the bright star, *r* = 13.04, ~25″ to the east of CXOJ1426+35, making this galaxy an ideal AO target.

Survey, an NOAO Large Survey Program (A. Gonzalez et al. 2011, in preparation). CXOJ1426+35 is detected in all bands. Table 1 lists the corresponding photometry in both Vega and AB magnitudes, where the latter assume the Vega–AB offsets from Blanton et al. (2005).

2.1.4. Mid-IR Imaging

CXOJ1426+35 has mid-IR data available from the *Spitzer* Deep, Wide-Field Survey (Ashby et al. 2009), a four-epoch infrared survey of 10 deg² in the Boötes field using the IRAC

(Fazio et al. 2004) on the *Spitzer Space Telescope*. Magnitudes are provided for channels 1, 2, 3, and 4, which correspond to bandpasses with effective wavelengths of 3.6, 4.5, 5.8, and 8.0 μm, respectively. The photometry listed in Table 1 assumes the position measured in the 4.5 μm image, and uses 4″0 radius aperture photometry, corrected to total magnitudes, and converted from Vega magnitudes to AB magnitudes using constants listed in the IRAC Data Handbook. The mid-IR colors are AGN-like, falling within the empirical separation of active galaxies from Galactic stars and normal galaxies (Stern et al. 2005), though it does lie on the red end of the overall AGN distribution.

2.1.5. Radio Imaging

CXOJ1426+35 is undetected in the deep, 1.4 GHz observation of the Boötes field by the Westerbork Synthesis Radio Telescope (de Vries et al. 2002). These data reach a median noise level of 140 μJy (5σ), and at this depth, no sources are detected within 14″6 of CXOJ1426+35. For a source at a redshift of $z = 1.175$, this detection limit corresponds to a radio power of $P_{1.4\,\mathrm{GHz}} = 1 \times 10^{23}$ W Hz^{-1}. For comparison, we used the 1.4 GHz radio powers of the 14 compact radio sources in Holt et al. (2008) (calculated using the published power-law indices) as those sources also exhibit narrow emission lines with velocity offsets, presumably as a result of interactions between the radio jets and the NLR clouds. The range of radio powers is $P_{1.4\,\mathrm{GHz}} = 3.8 \times 10^{26}$–$1.5 \times 10^{28}$ W Hz^{-1}, with a median of $P_{1.4\,\mathrm{GHz}} = 3.8 \times 10^{27}$ W Hz^{-1}, meaning this sample of compact radio sources would have all been detected in this observation. Therefore, CXOJ1426+35 is unlikely to be a similarly strong, compact radio source.

2.2. New Data and Analysis

While targeting a mid-IR transient which proved to be a self-obscured supernova at $z \sim 0.2$ (Kozłowski et al. 2010), we obtained a deep spectrum of CXOJ1426+35 at Keck Observatory in 2010 March. As described below, this intriguing spectrum triggered several additional observations.

2.2.1. Keck/LRIS: Optical Spectroscopy

Optical spectra of CXOJ1426+35 were obtained with the Low Resolution Imaging Spectrometer (LRIS; Oke et al. 1995) on UT 2010 March 12 using the D680 dichroic and the 400/3400 grism on the blue side and the 400/8500 grating on the red side. The 1″5 slit was oriented at position angle (P.A.) = $-21°$. The data consisted of three exposures of 1200 s each. For a 1″ slit, this instrument configuration provides a resolution of 6.5–7.1 Å (FWHM) on the blue side of the dichroic and 6.9 Å (FWHM) on the red side of the dichroic for objects filling the slit. We processed the data using standard techniques within IRAF. The two-dimensional spectra (Figure 3) show two emission line systems separated both spatially and along the dispersion axis. At a P.A. of $-21°$, the spatial separation is 0″48, as measured from the [Ne v]3426 line. To model the emission line velocity offsets and widths, we extracted an aperture of 3″ in diameter to recover the flux from the entire source (both emission line systems plus the continuum) and separate apertures centered on each component to isolate the flux from the "blue" and "red" systems. Figure 4 shows the 3″ extraction with the emission line identifications. These extractions mimic what an SDSS fiber spectrum of the source would look like, though the spatially resolved spectrum, shown in Figure 3, provides considerable additional information.

The extracted spectra were corrected for Galactic extinction using a color excess of $E(B - V) = 0.015$ determined from the model of Schlegel et al. (1998). We used SPECFIT (Kriss 1994) to model each emission line as two Gaussian profiles (for the "blue" and "red" emission line systems, respectively) on top of a local continuum. Unfortunately, the individual component apertures have significant contamination from each other, making it difficult to deconstruct the emission line flux attributable to each emission line system. Therefore, those apertures were used only to obtain estimates for the observed central wavelengths of each emission line, and the lines were fit again in the 3″ aperture to determine the spectral model parameters and associated errors. For the highly blended emission lines, some of the Gaussian parameters were fixed to those of less blended lines with similar ionization potentials (IPs). Doublets with rest wavelengths close together were modeled as single Gaussians. We also detected an absorption feature which is consistent with an H9 absorption line at a redshift intermediate to the two emission line systems. For each free parameter that was fit, the quoted errors correspond to 1σ uncertainties, and these errors were propagated into any further calculations. The line fluxes, FWHMs, redshifts, and velocities separations are presented in Table 2.

For both the "blue" and "red" systems each emission line is well fit by a single Gaussian. As measured from [Ne v]3426, the redshifts for the "blue" and "red" systems are $z = 1.1715$ and $z = 1.1773$, respectively. The range of spectral coverage is 3100–5200 Å on the blue side and 6700–9600 Å on the red side, which corresponds to rest-frame wavelength ranges of 1430–2380 Å and 3080–4410 Å and allows us access to a range of rest-frame optical and UV emission lines that are useful in diagnosing the structure and kinematics of the NLR gas from their velocities and line widths. If the absorption line is interpreted as H9 absorption within the host galaxy, this yields a systemic redshift of $z = 1.1751$. At this redshift, the emission line velocity splitting is 790 km s^{-1} as measured from [Ne v]3426. With no broad components detected in any of the optical/UV emission lines, the spectrum of CXOJ1426+35 resembles that of a Type 2 AGN, which in the unified theory of AGNs implies that the BLR and central continuum source are obscured. This is consistent with the heavy obscuration implied by the X-ray data.

2.2.2. Keck/NIRC2: Adaptive Optics Imaging

AO imaging of CXOJ1426+35 was obtained by the narrow camera of the Near-Infrared Camera 2 (NIRC2; van Dam et al. 2004) at the Keck II telescope on UT 2010 June 30. These data consisted of three 180 s data exposures at P.A. = 0°0 through the K' filter with an effective wavelength of $\lambda_{\mathrm{eff}} = 2.12\,\mu$m which corresponds to a rest-frame wavelength of $\lambda_{\mathrm{eff}} \sim 1\,\mu$m. An average dark field image was created using "imcombine" and was subtracted from each data image. Each image was flat fielded and then differenced from the other science frames. The images were shifted using the position of the target and then stacked using "imcombine." The final stacked image, 10″ on a side, is shown in Figure 5 and compared to the $g + r + i$ SDSS image and the Near-Infrared Spectrometer (NIRSPEC) image (see Section 2.2.3). The image reveals a single, diffuse source. The lack of two nuclei in the K' band implies that either there is no second AGN or alternatively that there is significant obscuration around 1 μm. Significant obscuration would also be consistent with the high column density implied by modeling of the X-ray data (Section 2.1.1) and with the extinction implied by our modeling of the SED (Section 2.3).
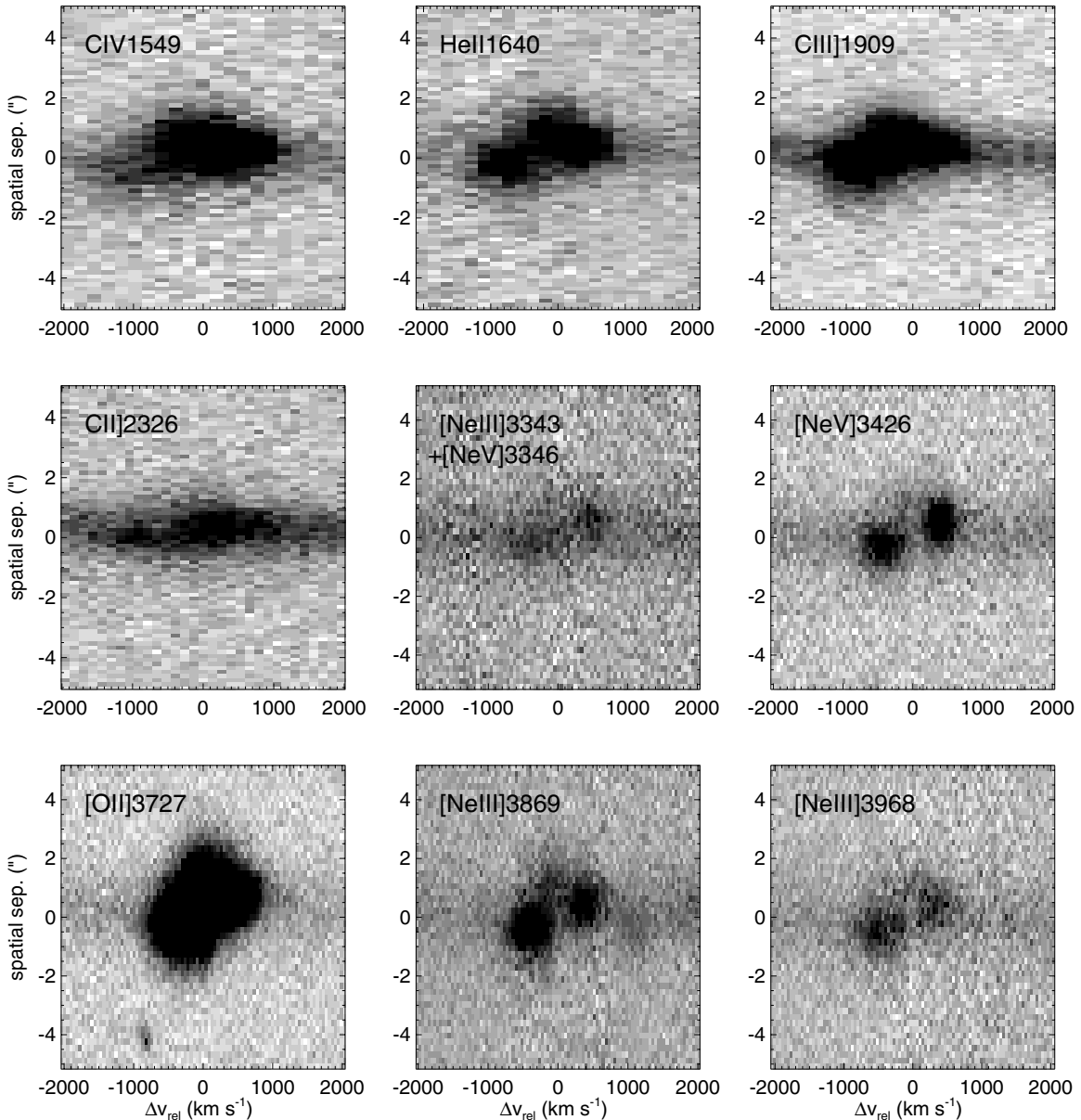
Figure 3. Prominent emission lines seen in the Keck/LRIS two-dimensional spectrum of CXOJ1426+35. The two components are most clearly seen in the forbidden lines which are narrower and less blended. For lines with blended doublets, particularly CIV1549 for which the "blue" component is much weaker than the "red," the two components are more difficult to resolve but still present. From left to right, the first four panels show emission lines from the blue side of the dichroic, and the last five panels are from the red side of the dichroic. The dispersion scale is 1.90 Å pixel^{-1} for the blue side and 1.18 Å pixel^{-1} for the red side. Note that the blue side was binned by two pixels in the dispersion direction. Along the spatial axis the scale is 0.135 arcsec pixel^{-1}. In each box the horizontal axis (relative velocity) spans 4000 km s^{-1} and the vertical axis (spatial separation along the slit) spans 10″. At a P.A. of $-21°$, the spatial separation between the two components is 0″48 and the velocity separation is 790 km s^{-1}, as measured from [Ne v]3426.

2.2.3. Keck/NIRSPEC: Near-IR Imaging and Spectroscopy

NIR imaging and spectroscopy of CXOJ1426+35 was obtained using the NIRSPEC (McLean et al. 1998) at the Keck II telescope on UT 2010 July 18.

Imaging. The imaging consisted of 11 dithered images of 10 s each. The filter used was the NIRSPEC-1 filter which has a wavelength range of 0.95–1.12 μm and is approximately a *Y*-band filter. The images were flat fielded and then differenced. The background was subtracted using "background" for each quadrant of each image independently and cosmic rays were removed using "xzap" in IRAF. The images were stacked with "imcombine" using for offsets the brightest star, when available, and the target otherwise. At a redshift of $z = 1.175$, the

filter provides rest-frame coverage of 0.44–0.52 μm. The final, combined image is presented in Figure 5 and reveals that the host galaxy dominates at optical wavelengths and consists of an elongated and "lumpy" structure that hints at a disturbed morphology.

Spectroscopy. We obtained NIRSPEC spectroscopy in low-resolution mode using a 0″7 wide slit placed at a position angle of P.A. $= -54°1$ so that the spatial axis was parallel to the major axis measured in the SDSS image. For a 0″38 slit, the spectrograph provides a resolving power of ∼2200. At two positions, A and B, along the slit, four 300 s exposures were taken in the order ABBA. The same filter as for imaging, NIRSPEC-1, was used. The spectra were differenced, cleaned of cosmic rays using the IRAF task "szap" and background
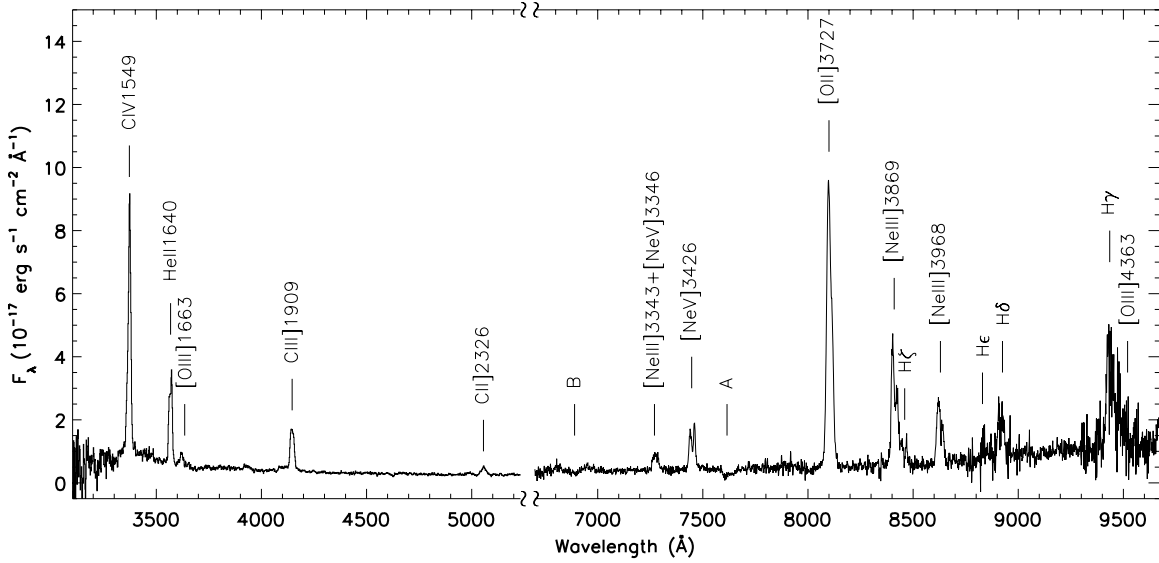
Figure 4. Keck/LRIS spectrum of CXOJ1426+35, in the observed frame, extracted from a 3″ diameter region including both velocity components, mimicking the source spectrum through an SDSS fiber. The emission lines and atmospheric absorption lines (A and B bands) are labeled. Note the double high-ionization narrow emission lines, suggestive of two Type 2 AGNs in the process of merging. Two-dimensional spectra of these emission lines are presented in Figure 3.
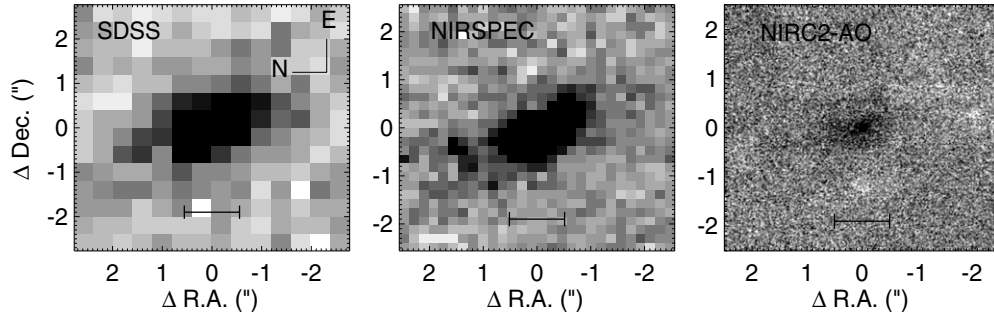

Figure 5. From left to right: stacked $g + r + i$ SDSS (0.40 arcsec pixel^{-1}), Y-band NIRSPEC (0.18 arcsec pixel^{-1}), and K'-band NIRC2-AO (0.01 arcsec pixel^{-1}) images. In each image, the scale bar represents 10 kpc at $z = 1.175$. The AO image has been smoothed by convolving with a Gaussian function using the "gauss" task in IRAF.

Table 2
Fluxes, FWHMs, Redshifts, and Velocity Splittings for Emission Lines in Both Systems

Line	Blue System			Red System			Velocity Splits
	Flux	FWHM	z	Flux	FWHM	z	
C IV 1549	23.30 ± 6.23	1120.95[a]	1.1718[c]	109.04 ± 9.85	1120.95 ± 85.65	1.1776	797.37 ± 75.49
He II 1640	20.70 ± 6.50	818.90 ± 162.03	1.1715	29.52 ± 6.58	872.33 ± 141.95	1.1779	882.47 ± 157.33
[O III]1663	1.65 ± 0.47	555.68[b]	1.1720[b]	3.10 ± 0.54	474.17[b]	1.1770[b]	690.95[b]
C III]1909	14.72 ± 6.19	925.58 ± 154.08	1.1687	14.34 ± 6.22	1003.31 ± 192.97	1.1745	971.68 ± 236.55
C II]2326	3.30 ± 1.90	880.83 ± 63.68	1.1718	2.32 ± 1.98	901.53 ± 239.35	1.7758	799.66 ± 462.92
[Ne v]3426	19.14 ± 1.25	590.33 ± 39.64	1.1715	17.48 ± 1.20	509.30 ± 36	1.1773	795.14 ± 28.90
[O II]3727	178.05 ± 76.04	719.33 ± 170.34	1.1722	80.10 ± 82.79	697.81 ± 237.48	1.1771	681.88 ± 333.59
[Ne III]3869	67.97 ± 5.73	615.60 ± 63.09	1.1718	37.06 ± 6.54	542.78 ± 97.99	1.1772	736.66 ± 49.73
[Ne III]3968	36.13 ± 2.27	615.60[c]	1.1718[c]	19.35 ± 1.61	542.78[c]	1.1772[c]	736.66[c]
Hγ	59.11 ± 8.21	587.03[d]	1.1724[d]	33.46 ± 6.39	474.17[d]	1.1766[d]	579.46[d]
[O III]4363	26.47 ± 5.04	555.68[b]	1.1720[b]	12.34 ± 3.46	474.17[b]	1.1770[b]	691.04[b]
Hβ	178.67 ± 63.15	587.03 ± 274.57	1.1724	⩽79.98	474.17[b]	1.1766	579.46 ± 156.43
[O III]4959	511.11 ± 108.30	487.90 ± 59.76	1.1721	186.61 ± 40.34	474.17[b]	1.1770[b]	675.94 ± 44.75
[O III]5007	1581.48 ± 132.82	555.68 ± 19	1.1720	477.93	474.17 ± 45.55	1.1770	690.95 ± 44.82

Notes. Fluxes are in units of 10^{-17} erg s^{-1} cm^{-2} Å^{-1}, and FWHMs and velocity splttings relative to $z = 1.175$ are in units of km s^{-1}. All errors correspond to 1σ uncertainties.
[a] Fixed to the "red" C IV 1549 component.
[b] Fixed to [O III]5007.
[c] Fixed to the value for [Ne III]3869.
[d] Fixed to the value for Hβ.

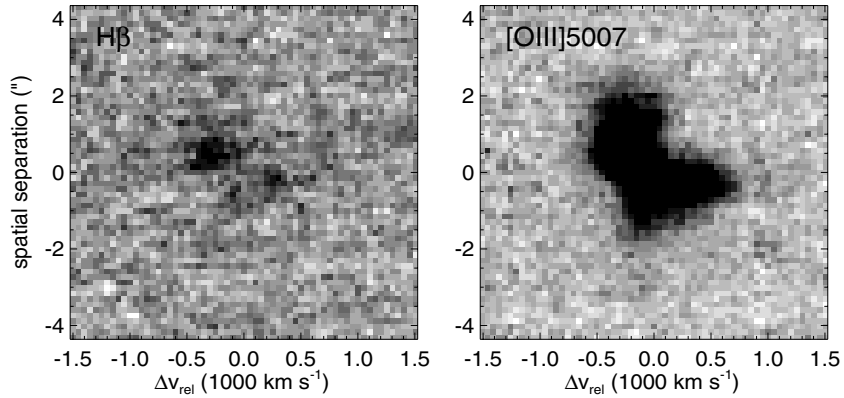**Figure 6.** Panel showing the Hβ and [O III]5007 emission lines in the two-dimensional NIRSPEC spectrum taken at P.A. of −54°.1. The dispersion scale is 2.10 Å pixel^{-1}, and the scale along the spatial axis is 0.143 arcsec pixel^{-1}. In each box the horizontal axis (relative velocity) spans 3000 km s^{-1} and the vertical axis (spatial separation along the slit) spans 9″. At P.A. of −54°.1 (aligned parallel to the major axis of the galaxy), the spatial separation between the two components is 0″.69 and the velocity separation is 690 km s^{-1}, as measured from [O III]5007.
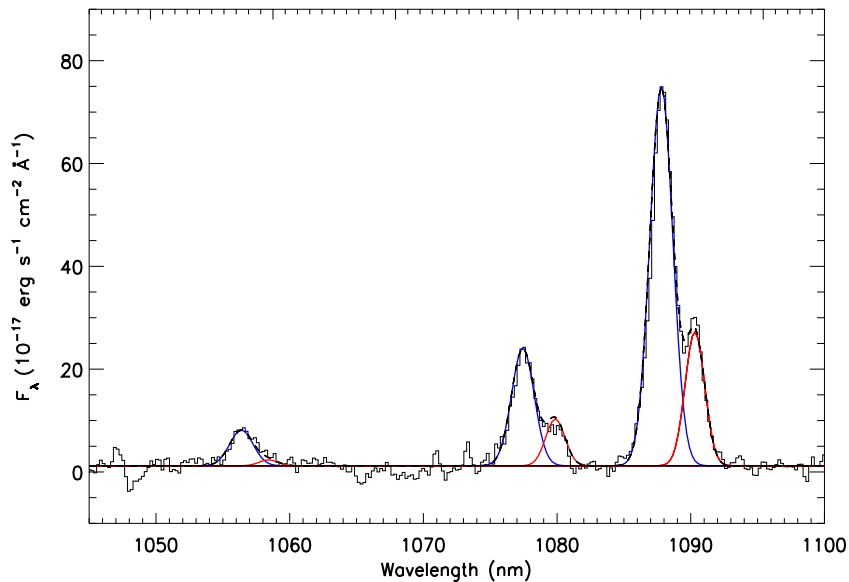
Figure 7. NIRSPEC spectrum of CXOJ1426+35, in the observed frame, extracted from an aperture 3″ in diameter that includes both velocity components. The emission lines are Hβ, [O III]4959, and [O III]5007. Overlaid on the spectrum are the best-fit Gaussians. Each emission line is fit by two Gaussians, one for the "blue" and one for the "red" emission line component.

(A color version of this figure is available in the online journal.)

subtracted using "background." The spectra were shifted and stacked using "imcombine."

The range of spectral coverage allows us access to the Hβ, [O III]4959, and [O III]5007 lines, which clearly show two emission line components (Figure 6). As measured from [O III]5007, the separation between the two components along the spatial axis (parallel to the major axis of the galaxy in the NIRSPEC image) is 0″.69. Aperture extractions and spectral modeling proceeded as with the LRIS spectrum. Three apertures were extracted that include a region of 3″ diameter encompassing the entire source and separate apertures for each of the "blue" and "red" systems. The extracted spectrum was corrected for Galactic extinction, and spectral modeling was performed on the 3″ aperture with "SPECFIT" with initial guesses for the line central wavelengths determined from the individual apertures for each component. The "red" Hβ component is very weak and therefore we have fixed its FWHM to that of the "red" [O III]5007 component and adopted the measured flux as an upper limit. Line fluxes, FWHMs, and

redshifts, and emission line velocity splittings are listed in Table 2.

The emission lines for both the "blue" and "red" systems are each fit by a single Gaussian (Figure 7). The [O III]5007 line has the highest S/N and the wavelength solutions for the Gaussian peaks provide a line-of-sight velocity separation of 690 km s^{-1}. The ratios between Hβ and Hγ are consistent within their errors with case B recombination theory for a reasonable NLR temperature range of 2500–20,000 K (Osterbrock & Ferland 2006). Considering the significant error of the Hγ flux measurement, we do not find any measurable Balmer decrement in the narrow emission line systems. The ratio between [O III]5007 and Hβ is highly useful in diagnosing the nature of the ionizing continuum through its placement on a BPT diagram (Baldwin et al. 1981). The line fluxes provide [O III]5007/Hβ ratios of 8.9 ± 3.2 for the "blue" system and a lower limit of 11.5 for the "red" system. Though we do not have access to Hα and cannot uniquely place the emission line systems on a typical diagnostic diagram (Kauffmann et al. 2003;
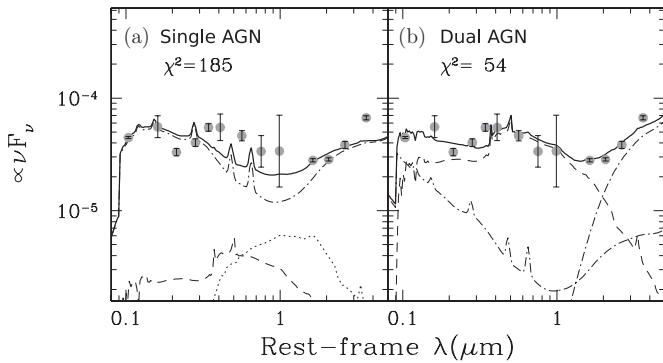
Figure 8. SED fits to the broadband photometry assuming a single (panel (a)) and dual (panel (b)) AGN components. The best-fit AGN components in each case are shown by the dot-dashed lines, while the Im component is shown by the dashed lines and the Sbc component is shown by the dotted lines (see Assef et al. 2010, for details on the SED templates). The solid line shows the best-fit SED, which corresponds to the addition of the different components.

Kewley et al. 2006), the [O III]5007/Hβ ratios put both systems above the demarcation defined in Kewley et al. (2001), clearly indicative of AGNs and consistent with the high-ionization lines observed in the optical spectrum.

2.3. Modeling of the Spectral Energy Distribution

Motivated by the high level of AGN obscuration implied from the X-ray HR and by the SDSS and NIRSPEC images, which suggest that the galaxy dominates at optical wavelengths, we have attempted to separate the SED into galaxy and AGN components to determine their relative contributions. This was done to determine if the AGN extinction inferred from the SED is consistent with the X-ray HR (Hickox et al. 2007) and, furthermore, if the SED is potentially consistent with two AGNs. We modeled the broadband photometry of CXOJ1426+35 using the SED templates for AGNs and galaxies of Assef et al. (2010). The four empirically constructed SED templates that form this basis extend from 0.03 to 30 μm and include an old stellar population (referred to as E), an intermediate star-forming population (Sbc), a strongly star-forming population (Im), and an AGN component. We refer the reader to Assef et al. (2010) for details on the SED templates. The standard approach of Assef et al. (2010) is to fit the broadband photometry with a non-negative linear combination of these four templates, allowing for additional dust extinction for the AGN component (and only the AGN component). However, this approach does not allow for a satisfactory fit to the broadband photometry ($\chi^2 = 185$; Figure 8(a)). Led by the possibility of CXOJ1426+35 being a dual AGN, we have modified our analysis and attempted to model the SED with two independent AGN components, each with a different amount of extinction, in addition to the host components. This approach yields a much better fit ($\chi^2 = 54$) as shown in Figure 8(b). An unreddened low-luminosity AGN component is used to model the UV excess over the galaxy-host SED, while another AGN component, intrinsically 10 times more luminous and with large amounts of obscuration ($E(B - V) = 3.44$), is used to model the mid-IR emission. This fit, while much better than that obtained with the standard approach of Assef et al. (2010), is still not completely satisfactory; the i band, which includes redshifted [O II]3727 emission, is underpredicted by $\sim3.5\sigma$ and the IRAC 8.0 μm band is underpredicted by $\sim4\sigma$. This does, however, lend credibility to the hypothesis that CXOJ1426+35 is a dual AGN. The SED modeling is compatible with the X-ray HR—the

color excess implies $n_H \approx 2 \times 10^{23}$ cm^{-2}, assuming an SMC-like gas/dust ratio (Maiolino et al. 2001)—and with the single source detected in the AO image, as the more luminous but highly reddened AGN component would dominate the X-ray emission but would be virtually invisible at rest-frame 1 μm ($A_{1\,\mu m} = 4.66$ mag from the extinction law of (Cardelli et al. 1989) and for $R_V = 3.1$.). The optical broad lines of the less luminous, unreddened AGNs (with $\sim10\%$ of the host luminosity) would be too faint to be detectable (Hopkins et al. 2009), consistent with our observations. We also find no significant evidence for a broad component in the UV lines, though in this model a broad component in C IV 1549 would possibly be detectable with sufficient signal quality. Furthermore, the relative luminosities of the two AGN components in the dual AGN model are consistent within the factor of four uncertainty of the bolometric luminosities, 5×10^{46} erg s^{-1} and 1.5×10^{46} erg s^{-1} for the "blue" and "red" components, respectively, from the $L_{[O\,III]}$ bolometric correction for Type 2 AGNs in Lamastra et al. (2009).

We note that an alternative approach would be to associate the UV excess with a very young stellar population instead of a second, lower luminosity AGN. Such a scenario would imply a star formation rate of approximately 40 $M_\odot$ yr^{-1} using the total UV luminosity at 2150 Å and the relation of Madau et al. (1998) for a Salpeter initial mass function and a stellar mass of approximately 10^{10} $M_\odot$ using the $g-r$ color and M/L_K relation of Bell et al. (2003) for the host. A specific star formation rate of $\sim4 \times 10^{-9}$ yr^{-1} is close to the high end of the distribution at the redshift of CXOJ1426+35 (see Cooper et al. 2008) but it is not implausibly large, making this modeling of the SED a viable alternative to the dual AGN scenario.

3. INTERPRETATION

In this section, we discuss six physical scenarios which may account for the unusual double emission line peaks observed in the rest-frame optical/UV lines, and the morphology as evident from the images, particularly the lack of a double nucleus in the NIRC2-AO image. These scenarios are a chance superposition, a rotating accretion disk, jet/cloud interactions, an unusual NLR geometry, accretion disk outflows, and a dual AGN. Similar explanations have been invoked for other dual AGN candidates and sources with double-peaked or offset emission lines (in particular, see the discussions of Gerke et al. 2007, Komossa et al. 2008a, and Xu & Komossa 2009), though we elaborate upon them here. We discuss the applicability of each scenario to CXOJ1426+35, concluding that a dual AGN is a viable explanation.

3.1. Superposition

A chance superposition of two unrelated sources has occasionally been posited as a possible interpretation of the multiple narrow emission lines seen in dual AGN candidates. Ignoring the fact that, in this case, the interpretation is rather forced since two systems with this little separation both physically and in velocity space are unlikely to be unrelated, we can use the surface density of AGNs to estimate the probability of such a chance superposition. Using the SDSS quasar catalog (Schneider et al. 2007) to determine the surface density of luminous (brighter than $M_i = -22.0$) quasars at $1.165 < z < 1.185$ (e.g., a redshift bin equivalent to nearly one hundred times the velocity difference between the two systems), we find a probability of $\sim3 \times 10^{-8}$ that CXOJ1426+35 is due to a chance superposition of field galaxies. We note that the SDSS quasars are luminous

Type 1 quasars and do not include obscured sources such as CXOJ1426+35. While this probability is small, it would increase were CXOJ1426+35 a member of a cluster (e.g., Dotti & Ruszkowski 2010). Using the cluster surface density at the high end of the surface density distribution in Dressler et al. (1997), we find that the probability increases by a factor of ~15, implying that even in a cluster this scenario is highly improbable.

3.2. Jet/Cloud Interaction

Radio jets produced by the central active SMBHs are capable of introducing a variety of kinematics into the NLR. Well-collimated jets can produce asymmetric and/or blueshifted narrow emission line profiles, and indeed jet/cloud interactions in the inner NLR have been used to explain the [O III] blueshifts seen in some compact radio sources (Holt et al. 2003, 2008; Fu & Stockton 2009). If the redshifted jet is not obscured, this scenario can explain the double-peaked narrow emission lines of CXOJ1426+35, and this was shown to be the case for a previous dual AGN candidate (Rosario et al. 2010). Nevertheless, some questions remain as to the capability of radio plasma to entrain the bulk of the NLR so that the velocity-shifted lines dominate in the emergent spectrum, rather than introduce instabilities that fragment the clouds. For example, Xu & Komossa (2009) discuss for another dual AGN candidate the scenario in which only a single cloud interacts locally with each side of the jet, but find that the [O III]5007 line luminosity is not consistent with just two clouds, and we arrive at the same conclusion for CXOJ1426+35 given its high [O III]5007 luminosity.

However, an even tighter constraint on the possibility of a jet/cloud interaction in CXOJ1426+35 is derived from the radio power corresponding to the radio detection limit (Section 2.1.5). The sample of radio sources in Holt et al. (2008) would have all been well detected. Though these are only 14 sources and do not represent all radio galaxies, they are useful for comparison as they show blueshifted [O III]5007 lines, presumably a result of local jet/cloud interactions in the inner NLR. If jet/cloud interactions are responsible for producing the double-peaked narrow emission lines, then CXOJ1426+35 is likely to be a strong radio source, similar to the radio sources in Holt et al. (2008), and would therefore have also been detected. However, the lack of a detection makes the presence of (at least strong) jet/cloud interactions highly unlikely.

3.3. Rotating Accretion Disk

A rotating disk with a line emitting surface is capable of producing double-peaked emission. The relative positions of the peaks and the shape of the lines are dependent on geometrical factors which can enhance the effect, such as the orientation of the disk plane relative to the observer's line of sight and the disk outer radius. Since this disk model has been successfully applied to accretion disks around SMBHs, providing a possible explanation for the asymmetric (non-Gaussian), broad, and often double-peaked Balmer emission lines of some AGNs and quasars, including some candidate binary SMBHs (see Section 1), we consider this scenario for CXOJ1426+35 but find that it is unlikely: the two-dimensional spectroscopy reveals that the line peaks are at a projected separation of ~5.5 kpc. This is much larger than the subparsec sizes of such disks based on SMBH masses and Hα line profiles (Chen & Halpern 1989) and makes the single accretion disk interpretation of CXOJ1426+35 unphysical.

3.4. Unusual NLR Geometry

One may imagine a disk-shaped NLR which can, in principle, produce the double-peaked lines in a way analogous to the rotating disk in Section 3.3. One advantage of this scenario is that NLRs are much larger than accretion disks and could explain the observed separation. While a size of 5.5 kpc is large for a typical Seyfert galaxy (Schmitt & Kinney 1996), luminous quasars have been observed with NLRs of up to 10 kpc (Bennert et al. 2002). The total [O III]5007 luminosity of CXOJ1426+35 is nearly an order of magnitude larger than that of the brightest quasar in the sample of Bennert et al. (2002), suggesting that the NLR of CXOJ1426+35 may plausibly extend to the observed separation of 5.5 kpc.

However, an additional and important consideration involves line ratios and line strengths: in this scenario both line systems should have similar line ratios and line strengths since the ionizing continuum incident on the gas and gas densities would be the same since they would be part of the same NLR. This scenario was found to be plausible for a subset of SDSS double-peaked AGN with even [O III] flux ratios in Smith et al. (2011). However, from Table 2, it is clear that the line ratios and line strengths, particularly for C IV1549 and [O III]5007, are not similar. Unless one side of the NLR suffers more extinction than the other, and there is no reason to expect this, the different line strengths are inconsistent with both line systems originating from the same classical NLR.

3.5. Accretion Disk Outflows

Winds moving in opposite directions and ionized by a central continuum source can, in theory, produce the double-peaked profile of the narrow emission lines (see the discussions in Xu & Komossa 2009 and Fischer et al. 2011). Mechanisms for producing such an outflow include radiation pressure acting on gas and dust (Everett 2007) or a hot wind that entrains the NLR clouds (Everett & Murray 2007). A potential problem with this scenario is the difficulty of the winds extending to typical NLR scales in order to affect the whole NLR. However, an SMBH accreting at a relatively high Eddington ratio ($f_{Edd} = L_{BOL}/L_{Edd}$) may be capable of producing a wind strong enough to extend to kpc scales. In general, luminous, Type 1 unobscured quasars at $z > 0.5$ may have typical Eddington ratios of $f_{Edd} \approx 0.25$ (Kollmeier et al. 2006), though recent work by Kelly et al. (2010) suggests that f_{Edd} peaks near 0.05, or alternatively AGNs might instead accrete close to Eddington in a "buried" phase as described in King (2010). In the sample of nine narrow line Seyfert 1 galaxies (NLS1s) with [O III] offsets in Komossa et al. (2008a) the Eddington ratios are high ($f_{Edd} = 0.5$–1.5, with the average value $f_{Edd} = 0.9$), and the authors remark that these high Eddington ratios may be capable of producing the strong outflows needed to explain the observed velocity shifts. In principle, a very rough estimate of the Eddington ratio can be made using the bolometric luminosity estimated in Section 2.1.1 and estimating an SMBH mass assuming all of the stellar mass (calculated in Section 2.3) is within the bulge and using the $M_{BH} \sim M_{Bulge}$ relation (Häring & Rix 2004). However, the resulting mass of $1.2 \times 10^7 \, M_\odot$ and the relation $L_{Edd} = 1.3 \times 10^{38} \, M_{BH}/M_\odot$ imply that the bolometric luminosity is ~50 times that of the Eddington limit. This result seems unphysical, possibly because this galaxy is still in the process of forming and the $M_{BH} \sim M_{Bulge}$ relation has yet to be established in this system. The optical/UV emission lines may be used as diagnostic
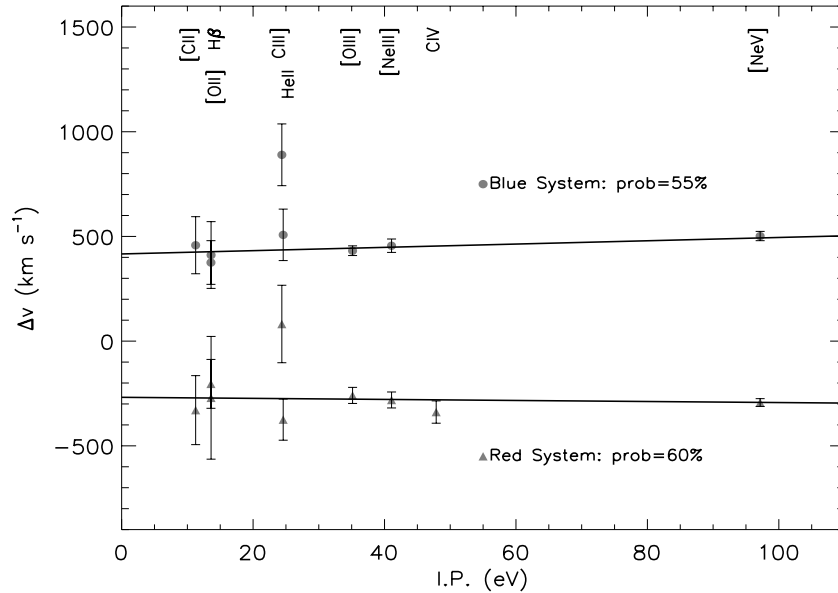
Figure 9. Plot of emission line velocity splittings for the "blue" and "red" systems relative to $z = 1.1751$ (i.e., the systemic velocity as measured from the H9 absorption line in Section 2.2.1), where positive velocities indicate a blueshift. The plotted data points correspond to emission lines for which the positions were allowed to vary during the fit. Some of the line labels have been shifted for clarity. The straight lines are the linear least-squares best fits. The quoted probabilities for each system are the two-sided significances, based on a Spearman rank correlation, of the deviation from the null hypothesis that there is no evolution of ΔV with IP. In both systems, the probabilities provide no indication of a correlation. The apparent blueshift of C III]1909 in each system may be the result of an increase in the $I(\lambda1907)/I(\lambda1909)$ ratio (see Section 3.5).

indicators of the ionization parameters and kinematics of the "blue" and "red" systems. We perform two calculations based upon the emission line parameters that provide clues as to the origin of the double-peaked lines.

Ionizing continuum. We can use the ionizing continuum to estimate the maximum distance at which the emission line regions can be so ionized to determine if the outflow scenario is plausible. The ionizing continuum is described by $Q[H^0]$, which we have estimated from the total Hβ luminosity of both the "blue" and "red" sources via the relation $L_{H\beta} = h\nu_{H\beta}(\alpha_{H\beta}^{eff}/\alpha_B)(\Omega/4\pi)Q[H^0]$. The expected distance can then be found from the relation $U = Q[H^0]/(4\pi r^2 c n_H)$, where U is the ionization parameter estimated as a function of gas density from the [O II]3727/[O III]5007 ratios (Komossa et al. 2006). The calculated distances are highly dependent on the global covering factor, Ω, of the winds as viewed from the central source. Therefore, we adopt a lower limit of $\Omega = 1.6$ (Blustin & Fabian 2009) for each source, which corresponds to an upper limit on the distances. Assuming a pure hydrogen nebula and complete ionization ($n_H = n_e$), we estimate the distances for a typical range of NLR electron densities ($n_e = 10^2$–10^4 cm^{-3}), where 10^4 cm^{-3} is an upper limit based on the critical density for de-excitation of [O II]3727, which is well detected in the spectrum of CXOJ1426+35. Given the range in electron densities, we find maximum distances of 2–5 kpc and 2–6 kpc for which the "blue" and "red" systems, respectively, can be so ionized. While these distances are consistent with the projected separation of 5.5 kpc, making the outflow scenario plausible on these grounds, it should be noted that these estimates are intended as upper limits and that the projected separation is a lower limit on the actual physical separation. Therefore, these calculations merely show that within the uncertainties of the geometry of the system, two clouds with the observed [O II]3727/[O III]5007 line ratios and Hβ luminosities could be ionized by a single source. The limits of this argument are apparent when one considers the significantly different line

ratios and line strengths between the two systems as noted in Section 3.4. In particular, the significantly different C IV1549 and [O III]5007 strengths are not expected if the outflowing clouds are at the same distance from the AGNs and have similar compositions. However, in principle, a clumpy obscuring geometry could account for this observation.

Ionization stratification. The outflow scenario should produce a positive correlation between IP and velocity offset, ΔV, otherwise known as an "ionization stratification." This is because the high-ionization lines will originate closer to the central source where the flux is large enough to produce such lines, whereas low-ionization lines will originate further out where they are less affected by the outflow. Such a line stratification is evident in the sample of NLS1s with blueshifted [O III]5007 lines from Komossa et al. (2008a). We investigate ΔV versus IP for CXOJ1426+35 using the emission lines for which the central wavelength was allowed to vary during the fitting procedure. From a Spearman rank correlation test, we find probabilities for a correlation between IP and ΔV of 55% and 60% for the "blue" and "red" systems, respectively. These probabilities indicate that a significant correlation is not apparent given the available line measurements. In Figure 9, we plot ΔV versus IP for each system along with the linear least-squares best fit. In both systems, the velocities are all consistent within their errors, with the exception of C III]1909. Since the C III]1909 apparent blueshift appears in both systems it may be related to the anomalous C III]1909 blueshift seen in some quasars as a result of the increased intensity of the $\lambda1907$ transition relative to $\lambda1909$ ($\sim$300 km s^{-1} offset) at low densities (Ferland 1981). While there is no apparent correlation, it should be noted that in the Komossa et al. (2008a) sample, two galaxies have the [Fe x] line from the coronal line region (IP = 235 eV), significantly higher than the highest IP line observed for CXOJ1426+35 ([Ne v], IP = 97 eV). For the four NLS1s in that sample that do not include the [Fe x] line, the trends are comparable to that of CXOJ1426+35. This indicates there is a possibility that a

line stratification might become apparent with a wider range of IPs.

3.6. Galaxy Merger and Dual SMBHs

A system of two SMBHs within the host galaxy, with at least one of them active, would naturally explain the two emission line systems as each SMBH would provide its own NLR. Since such a system would arise from a galaxy merger, one may speculate that it is more likely to be found in a disturbed system. Indeed, the morphology of CXOJ1426+35, particularly the "lumpy" structure evident in the NIRSPEC image in Figure 5, suggests a possible disturbance of some kind. This possibility seems even more likely when one considers that, at $z = 1.175$, galaxy mergers were more frequent than in the local universe (Bridge et al. 2010). We also speculate that the X-ray spectrum (which implies a high level of dust extinction) is indicative of a galaxy that has recently undergone a merger. Therefore, the interpretation of CXOJ1426+35 hosting two SMBHs is quite plausible and worthy of consideration. We consider two possibilities involving a galaxy merger and formation of a dual SMBH system.

One AGN illuminating two NLRs. This scenario was also suggested for a candidate dual SMBH in Xu & Komossa (2009). It is possible that after the merger, only one of the SMBHs would be active but both would have their own NLR. The active AGN may therefore be able to ionize both NLRs which would have a velocity difference imparted to them by the merger. For the NLR around the inactive SMBH, assuming it is completely ionized by the active SMBH and with $n_e = 10^2$ cm^{-3}, we estimate a free-fall timescale of $\sim 5 \times 10^6$ years. This is a relatively short time, and it is unlikely that we would see the system during this window. However, a more rigorous test for this scenario uses the expectation that the ionization parameter and hydrogen number densities should be consistent with one NLR being further from the ionizing source than the other. In Section 3.5, we estimated a range of distances based on the ionization parameters (estimated from the [O II]3727/[O III]5007 ratio) and a typical range of electron densities ($n_e = 10^2$–10^4 cm^{-3}). It is theoretically possible to obtain an independent estimate for the electron densities of each emission line system from the flux ratios of emission lines produced by different transitions within the same ion, particularly [O III]($j_{\lambda 4959} + j_{\lambda 5007}$)/$j_{\lambda 4363}$ and assuming a temperature of the gas (Osterbrock & Ferland 2006). However, while the measured [O III] ratios are well within the typical values for AGN NLRs, we note that n_e is strongly dependent on the NLR temperature, and photoionization models imply NLRs may have multiple zones with different temperatures and densities (Krolik 1999). Therefore, we have chosen to simply use the typical range of densities in our estimates. Given the range of distances for each system, the possible ratios between the distance of the "blue" component to that of the "red" component range from 1:3 to 2.5:1. In no case does the ratio of distances imply one source is significantly further than the other, providing no strong evidence for just one source being associated with an AGN.

Two AGNs. It is generally agreed that galaxy mergers, through tidal interactions, are effective at enhancing SMBH activity by funneling gas and dust toward the central region of the new distribution of mass (Hernquist 1989; Springel et al. 2005). Therefore, if CXOJ1426+35 did experience a wet merger, then the merger would have increased the probability for the two SMBHs to be active as gas would be funneled toward the potential well of each SMBH. On these grounds a dual AGN

scenario is highly plausible and would naturally explain the two emission line systems. A potential piece of evidence against this hypothesis is the NIRC2-AO image which reveals only one source at rest-frame 1μm as opposed to the two nuclei expected in the dual AGN scenario. However, there are several properties of CXOJ1426+35 which point to a high level of internal extinction capable of obscuring an AGN continuum at rest-frame 1μm. In particular, the high X-ray HR implies there is at least one AGN suffering significant absorption, e.g., $n_H = 6 \times 10^{23}$ cm^{-2} (Section 2.1.1) and modeling of the SED (Figure 8) reveals that an AGN with comparable absorption would be virtually invisible at rest-frame 1μm (Section 2.3). This AGN would dominate in the X-ray and IRAC bands, while a second, less obscured AGN would be associated with the source seen at 1μm. We note that another candidate dual AGN (Comerford et al. 2011) also shows only a single component in AO imaging, but which may host two heavily obscured (Compton thick) AGNs as revealed from *Chandra* data. As discussed in Section 1, several confirmed that dual AGNs (Guainazzi et al. 2005; Bianchi et al. 2008; Piconcelli et al. 2010; Koss et al. 2011) provide examples of this scenario, showing only one visible nucleus, with the other heavily obscured and identifiable only through X-ray observations. Given the prevalence of heavy obscuration in other candidate and confirmed dual AGNs, the lack of detection of two cores would not be surprising if CXOJ1426+35 in fact hosted a dual AGN.

3.7. Multiple Scenarios

Finally, we note that more than one of these physical mechanisms may be present. In particular, we note the possible coexistence of a galaxy merger and AGN outflows. This follows from the morphology of CXOJ1426+35, which suggests a possible merger, and from the notion that galaxy mergers are potential instigators of enhanced SMBH activity. If the merger has resulted in an AGN with a relatively high Eddington ratio (e.g., >0.25 and perhaps close to the Eddington limit), the accretion disk radiation pressure may be capable of producing the double-peaked narrow lines as discussed in Section 3.5. While an ionization stratification is not apparent given the current data, we could not rule one out for either system. This scenario is consistent with both the morphological suggestion of a recent merger while allowing for the existence of strong outflows driven by the radiation pressure of AGN accretion disks.

3.8. Summary

We have discussed six separate physical mechanisms that are each capable of producing double-peaked emission lines and we have discussed the likelihood of each scenario based on the available data. We find that a superposition, even within a galaxy cluster, is highly unlikely given the small physical and velocity separation and that the rotating accretion disk scenario is highly unlikely given the several kiloparsec separation. We find that a jet/cloud interaction is also highly unlikely simply because it is not a strong radio source. The scenario of an NLR with an disk-shaped component can naturally explain the double peaks, but the disagreement between the line ratios and line strengths of both systems is not expected in that scenario. We find that the biconical outflow from an accretion disk cannot be ruled out and that the primary limitation is the power of the accretion disk. A recent galactic merger would potentially make the biconical outflow a more likely explanation, although there is no clear line

stratification. In the case of a single AGN, the SED modeling implies there might also be very young stellar population present which accounts for the UV excess. A merger would also increase the possibility of a single AGN illuminating the NLR of each galaxy, though this scenario may not be likely given the short free-fall timescale and the similar distances of each cloud based on a single ionizing source. A more likely scenario is that there are actually two AGNs present. The lack of two nuclei in the NIR AO image provides possible evidence against a second AGN, but this may be naturally explained by the high obscuration, inferred from both the X-ray data and the SED modeling, which would obscure the continuum radiation. This scenario is also consistent with the several kiloparsec separation of the AGN components, since many of the dual AGNs already identified have comparable separations, and it is consistent with the AGN-like line ratios.

4. TESTS FOR DUAL AND BINARY SMBHs

Based upon limited data, determining the true nature of many candidate dual and binary SMBH systems has proven to be difficult given the attractiveness of alternative explanations. Among the current handful of candidates there is a variety of data and interpretations, many of which have been tested and often with ambiguous results. Here we use CXOJ1426+35, in comparison with other candidates, to review how these candidates can be tested.

4.1. One-dimensional Spectroscopy

Given the availability of spectroscopic databases that include large samples of AGNs and quasars, emission line diagnostics are commonly used to select the most promising double-peaked emission line candidates for follow-up observations. From one-dimensional spectra alone (i.e., SDSS fiber spectra), much can be done to address the likelihood of a dual/binary AGN. Emission line ratios can provide information about the source of the ionizing continuum radiation (Baldwin et al. 1981; Kauffmann et al. 2003), and careful examination of spectra may also reveal asymmetries, velocity offsets, or multiple components, thereby providing valuable information about the kinematics of the NLR gas. We have performed these analyses for CXOJ1426+35 in the above discussion, and they have been done for all of the other candidate dual/binary SMBHs yet identified, providing valuable information and resulting in a variety of interpretations. For example, in J0927+2943, close examination of the optical spectra (which features two prominent emission line systems, one with just narrow lines and the other with broad and narrow lines) has allowed for multiple models to be put forth, including a recoiling SMBH (Komossa et al. 2008b), a binary SMBH (Bogdanović et al. 2009b; Dotti et al. 2009), a superposition (Shields et al. 2009a), and a large and small galaxy interacting near the center of a rich cluster (Heckman et al. 2009). As another example, in J1316+1753 Xu & Komossa (2009) identified two NLRs and at an intermediate redshift there is a broad component to each emission line, which the authors discuss may be evidence of a starburst-driven outflow that was triggered by a merger.

We also note that spectroscopic observations over multiple epochs could potentially reveal any orbital motion in a close binary SMBH system. Though CXOJ1426+35 does not fall into this class as the implied separation is much too large, candidate close binary SMBHs could be identified in this manner. This test has been performed for both J0927+2943 (Vivek et al. 2009)

and J1536+0441 (Chornock et al. 2010) which were identified as candidate subparsec binaries with separations of ~0.34 pc (Dotti et al. 2009) and ~0.1 pc (Boroson & Lauer 2009), respectively. In both cases, the acceleration is found to be zero within the errors. However, it has been pointed out that such candidates would be preferentially identified when their radial velocities are largest and the radial accelerations smallest (Bogdanović et al. 2009a).

4.2. Two-dimensional Spectroscopy

By providing information about the spatial separation of the two emission line components, two-dimensional spectroscopy has proven to be highly effective at identifying the most promising dual AGN candidates from the much larger sample of double-peaked narrow emission line sources. In this way, CXOJ1426+35 has been shown to be a strong dual AGN candidate based on the two emission line components spatially separated and with a velocity difference of several hundred km s^{-1}. At lower redshifts, there are many other similar candidates for which two-dimensional spectroscopy reveals two clearly separated components (e.g., Comerford et al. 2009b, 2009a). Two-dimensional spectroscopy ruled out the close binary hypothesis for J0927+2943, but showed that it may still be a system of two merging galaxies (Vivek et al. 2009). A large sample of double-peaked AGNs with follow-up two-dimensional spectroscopy will increase the number of candidate dual AGNs (Comerford et al. 2011, in preparation). However, as made evident in our analysis of CXOJ1426+35, two-dimensional spectroscopy alone cannot confirm a dual AGN.

4.3. Morphology

Morphology can provide powerful evidence for or against the dual AGN hypothesis. A number of objects which show double-peaked emission lines have been imaged in optical- and near-IR bands, where the results have shown morphological evidence of interactions/mergers such as tidal tails and multiple nuclei (Junkkarinen et al. 2001; Comerford et al. 2009a; Green et al. 2010; Liu et al. 2010a). From *Hubble Space Telescope* (*HST*) imaging, the galaxy COSMOS J100043.15+020637.2 has been established as hosting either a dual (Comerford et al. 2009b) or a recoiling SMBH (Civano et al. 2010). In the case of EGSD2 J142033.66+525917.5 (Gerke et al. 2007), an *HST* Advanced Camera for Surveys image shows morphological evidence of a possible interaction, but no clear evidence for multiple nuclei. Rosario et al. (2011) and Shen et al. (2011) have obtained NIR imaging of several [O III] double-peaked AGNs where the results have shown a variety of possible origins of the double-peaked narrow emission lines, including some sources with morphological evidence suggesting the most likely interpretation is a dual AGN. Fu et al. (2011) present images for a sample of several such candidates which reveal multiple nuclei in some cases, though they caution that spatially resolved spectroscopy is required to confirm any case as a true dual AGN. In McGurk et al. (2011) integral field spectroscopy was able to confirm a dual AGN. That source was confirmed in the same way in Fu et al. (2011), though their sample revealed that, out of 42 sources, in all but two the double-peaked lines were produced by gas kinematics. These studies have highlighted the usefulness of integral field spectroscopy in eliminating the ambiguities left by double-peaked emission lines and even high-resolution imaging. In the case of CXOJ1426+35, NIR AO imaging revealed only a single nucleus at a rest-frame effective wavelength of 1 μm,

providing possible evidence against the dual AGN scenario. As with other dual AGN candidates, integral field spectroscopy will be useful for CXOJ1426+35.

In the case of heavy nuclear obscuration, however, detection of double point sources in X-ray images of close ULIRGs has been effective at identifying dual AGN, e.g., NGC 6240 (Komossa et al. 2003), ESO509-IG066 (Guainazzi et al. 2005), 3C 75 (Hudson et al. 2006), Mrk 436 (Bianchi et al. 2008), and IRAS 20210+1121 (Piconcelli et al. 2010). The advantage of this method of detection is that hard X-rays are much less attenuated by intervening material in the galaxy and recent mergers are known to have high column densities in the nuclear regions. This might be the case for CXOJ1426+35, as dust may have a strong role in hiding an AGN near $1 \mu m$, whereas two AGNs would be revealed from hard X-rays. Though CXOJ1426+35 is unresolved in our image, this is due to the off-axis detection and the resolution of the ACIS detector. With the High Resolution Camera, the two X-ray components could potentially be resolved in CXOJ1426+35.

5. CONCLUSIONS

We have analyzed all available data, new and archival, of the source CXOJ1426+35 which has an intriguing spectrum showing double-peaked optical/UV emission lines. The two emission line components, separated spatially by $0''.69$ (5.5 kpc) and in velocity space by 690 km s^{-1}, make CXOJ1426+35 similar to other candidate dual AGNs, though it is unique in that it is the highest redshift candidate dual AGN yet identified. The optical/NIR imaging shows an elongated and "lumpy" morphological structure suggestive of a disturbance, whereas the AO image shows only a single source. We have discussed several interpretations of the physical nature of CXOJ1426+35, including a chance superposition, a jet/cloud interaction, line emission from a rotating accretion disk, an unusual NLR geometry, a strong biconical outflow from an accretion disk, a dual SMBH, and a combination of these scenarios. We find that the only plausible scenarios are a strong outflow, a dual SMBH system, or a combination thereof. If CXOJ1426+35 recently underwent a merger, an increased Eddington ratio may have resulted, making the disk outflow scenario a possible explanation. Alternatively, a merger may have resulted in the actual case of a dual AGN, or, less likely, a single AGN illuminating the NLRs of both SMBHs. Regardless, CXOJ1426+35 is most likely a merger remnant.

Finally, we compared CXOJ1426+35 to other candidates with the aim of reviewing methods of testing the dual AGN hypothesis. Analysis of single-epoch one-dimensional and two-dimensional spectra provides crucial information about the ionizing continuum and the velocity and spatial separation of the two emission line components, but multi-epoch spectra and high-resolution imaging have proven most effective at confirming or rejecting the dual/binary SMBH hypothesis. CXOJ1426+35 represents an interesting example of a dual AGN candidate, with many properties similar to other candidates in the literature, but also with several unique characteristics. In particular, CXOJ1426+35 is the highest redshift dual AGN candidate to-date, at a redshift of $z = 1.175$ when galaxy mergers were more frequent, making the dual AGN hypothesis especially appealing. This makes it a fascinating addition and will help in developing a better understanding of how to look for the potential signatures of dual/binary SMBHs and of the often complex emission line regions of AGNs.

REFERENCES

Abazajian, K. N., Adelman-McCarthy, J. K., Agüeros, M. A., et al. 2009, ApJ, 182, 543
Ashby, M. L. N., Stern, D., Brodwin, M., et al. 2009, ApJ, 701, 428
Assef, R. J., Kochanek, C. S., Brodwin, M., et al. 2010, AJ, 713, 970
Baldwin, J. A., Phillips, M. M., & Terlevich, R. 1981, PASP, 93, 5
Barrows, R. S., Lacy, C. H. S., Kennefick, D., Kennefick, J., & Seigar, M. S. 2011, New Astron., 16, 122
Begelman, M. C., Blandford, R. D., & Rees, M. J. 1980, Nature, 287, 307
Bell, E. F., McIntosh, D. H., Katz, N., & Weinberg, M. D. 2003, ApJS, 149, 289
Bennert, N., Falcke, H., Schulz, H., Wilson, A. S., & Wills, B. J. 2002, ApJ, 574, L105
Bianchi, S., Chiaberge, M., Piconcelli, E., Guainazzi, M., & Matt, G. 2008, MNRAS, 386, 105
Blanton, M. R., Schlegel, D. J., Strauss, M. A., et al. 2005, AJ, 129, 2562
Blustin, A. J., & Fabian, A. C. 2009, MNRAS, 396, 1732
Bogdanović, T., Eracleous, M., & Sigurdsson, S. 2009a, New Astron., 53, 113
Bogdanović, T., Eracleous, M., & Sigurdsson, S. 2009b, ApJ, 697, 288
Bohlin, R. C., Dickinson, M. E., & Calzetti, D. 2001, AJ, 122, 2118
Boroson, T. A., & Lauer, T. R. 2009, Nature, 458, 53
Bridge, C. R., Carlberg, R. G., & Sullivan, M. 2010, ApJ, 709, 1067
Cardelli, J. A., Clayton, G. C., & Mathis, J. S. 1989, ApJ, 345, 245
Chen, K., & Halpern, J. P. 1989, ApJ, 344, 115
Chornock, R., Bloom, J. S., & Cenko, S. B. 2010, ApJ, 709, L39
Civano, F., Elvis, M., Lanzuisi, G., et al. 2010, ApJ, 717, 209
Comerford, J. M., Gerke, B. F., Newman, J. A., et al. 2009a, ApJ, 698, 956
Comerford, J. M., Griffith, R. L., Gerke, B. F., et al. 2009b, ApJ, 702, L82
Comerford, J. M., Pooley, D., Gerke, B. F., & Madejski, G. M. 2011, ApJ, 737, L19
Cooper, M. C., Tremonti, C. A., Newman, J. A., & Zabludoff, A. I. 2008, MNRAS, 390, 245
Daly, R. A. 1992, ApJ, 399, 426
de Vries, W. H., Morganti, R., Röttgering, H. J. A., et al. 2002, AJ, 123, 1784
De Young, D. S. 1981, Nature, 293, 43
Decarli, R., Dotti, M., Montuori, C., Liimets, T., & Ederoclite, A. 2010, ApJ, 720, L93

Dotti, M., Montuori, C., Decarli, R., et al. 2009, MNRAS, 398, L73
Dotti, M., & Ruszkowski, M. 2010, ApJ, 713, L37
Dressler, A., Oemler, A., Jr., Couch, W. J., et al. 1997, ApJ, 490, 577
Everett, J. E. 2007, Ap&SS, 311, 269
Everett, J. E., & Murray, N. 2007, ApJ, 656, 93
Fazio, G. G., Hora, J. L., Allen, L. E., et al. 2004, ApJS, 154, 10
Ferland, G. J. 1981, ApJ, 249, 17
Fischer, T. C., Crenshaw, D. M., Kraemer, S. B., et al. 2011, ApJ, 727, 71
Foreman, G., Volonteri, M., & Dotti, M. 2009, ApJ, 693, 1554
Fu, H., Myers, A. D., Djorgovski, S. G., & Yan, L. 2011, ApJ, 733, 103
Fu, H., & Stockton, A. 2009, ApJ, 690, 953
Fu, H., Yan, L., Myers, A. D., et al. 2011, arXiv:1107.3564
Garmire, G. P., Bautz, M. W., Ford, P. G., Nousek, J. A., & Ricker, G. R., Jr.
    2003, Proc. SPIE, 4851, 28
Gerke, B. F., Newman, J. A., Lotz, J., et al. 2007, ApJ, 660, L23
Green, P. J., Myers, A. D., Barkhouse, W. A., et al. 2010, ApJ, 710, 1578
Guainazzi, M., Piconcelli, E., Jiménez-Bailón, E., & Matt, G. 2005, A&A, 429,
    L9
Häring, N., & Rix, H. 2004, ApJ, 604, L89
Heckman, T. M., Krolik, J. H., Moran, S. M., Schnittman, J., & Gezari, S.
    2009, ApJ, 695, 363
Heckman, T. M., Miley, G. K., van Breugel, W. J. M., & Butcher, H. R.
    1981, ApJ, 247, 403
Hennawi, J. F., Myers, A. D., Shen, Y., et al. 2010, ApJ, 719, 1672
Hennawi, J. F., Strauss, M. A., Oguri, M., et al. 2006, AJ, 131, 1
Hernquist, L. 1989, Nature, 340, 687
Hickox, R. C., Jones, C., Forman, W. R., et al. 2007, ApJ, 671, 1365
Holt, J., Tadhunter, C. N., & Morganti, R. 2003, MNRAS, 342, 227
Holt, J., Tadhunter, C. N., & Morganti, R. 2008, MNRAS, 387, 639
Hopkins, P. F., Hernquist, L., Cox, T. J., & Kereš, D. 2008, ApJS, 175, 356
Hopkins, P. F., Hernquist, L., Cox, T. J., et al. 2005, ApJ, 630, 705
Hopkins, P. F., Hickox, R., Quataert, E., & Hernquist, L. 2009, MNRAS, 398,
    333
Hopkins, P. F., Richards, G. T., & Hernquist, L. 2007, ApJ, 654, 731
Hudson, D. S., Reiprich, T. H., Clarke, T. E., & Sarazin, C. L. 2006, A&A, 453,
    433
Jannuzi, B. T., & Dey, A. 1999, in ASP Conf. Ser. 191, Photometric Redshifts
    and the Detection of High Redshift Galaxies, ed. R. Weymann et al. (San
    Francisco: ASP), 111
Junkkarinen, V., Shields, G. A., Beaver, E. A., et al. 2001, ApJ, 549, L155
Kauffmann, G., Heckman, T. M., Tremonti, C., et al. 2003, MNRAS, 346, 1055
Kelly, B. C., Vestergaard, M., Fan, X., et al. 2010, ApJ, 719, 1315
Kewley, L. J., Dopita, M. A., Sutherland, R. S., Heisler, C. A., & Trevena, J.
    2001, ApJ, 556, 121
Kewley, L. J., Groves, B., Kauffmann, G., & Heckman, T. 2006, MNRAS, 372,
    961
King, A. R. 2010, MNRAS, 408, L95
Kollmeier, J. A., Onken, C. A., Kochanek, C. S., et al. 2006, ApJ, 648, 128
Komossa, S., Burwitz, V., Hasinger, G., et al. 2003, ApJ, 582, L15
Komossa, S., Voges, W., Adorf, H., et al. 2006, ApJ, 639, 710
Komossa, S., Xu, D., Zhou, H., Storchi-Bergmann, T., & Binette, L. 2008a, ApJ,
    680, 926
Komossa, S., Zhou, H., & Lu, H. 2008b, ApJ, 678, L81
Koss, M., Mushotzky, R., Treister, E., et al. 2011, ApJ, 735, L42
Kozłowski, S., Kochanek, C. S., Stern, D., Prieto, J. L., & Stanek, K. Z. 2010,
    CBET, 2392, 1
Kriss, G. 1994, in ASP Conf. Ser. 61, Astronomical Data Analysis Software
    and Systems, Vol. 3, ed. D. R. Crabtree, R. J. Hanisch, & J. Barnes (San
    Francisco, CA: ASP), 437
Krolik, J. H. (ed.) 1999, Active Galactic Nuclei: From the Central Black Hole
    to the Galactic Environment (Princeton, NJ: Princeton Univ. Press)

Kurucz, R. L. 1993, VizieR Online Data Catalog, 6039, 0
Lamastra, A., Bianchi, S., Matt, G., et al. 2009, A&A, 504, 73
Liu, X., Greene, J. E., Shen, Y., & Strauss, M. A. 2010a, ApJ, 715, L30
Liu, X., Shen, Y., Strauss, M. A., & Greene, J. E. 2010b, ApJ, 708, 427
Madau, P., Pozzetti, L., & Dickinson, M. 1998, ApJ, 498, 106
Maiolino, R., Marconi, A., Salvati, M., et al. 2001, A&A, 365, 28
Martin, C., Barlow, T., Barnhart, W., et al. 2003, Proc. SPIE, 4854, 336
Maxfield, L., Spinrad, H., Stern, D., Dey, A., & Dickinson, M. 2002, AJ, 123,
    2321
McCarthy, P. J. 1993, ARA&A, 31, 639
McGurk, R. C., Max, C. E., Rosario, D. J., et al. 2011, ApJ, 738, L2
McLean, I. S., Becklin, E. E., Bendiksen, O., et al. 1998, Proc. SPIE, 3354, 566
Miley, G., & De Breuck, C. 2008, A&AR, 15, 67
Milosavljević, M., & Merritt, D. 2003, ApJ, 596, 860
Morrissey, P., Conrow, T., Barlow, T. A., et al. 2007, ApJS, 173, 682
Myers, A. D., Brunner, R. J., Richards, G. T., et al. 2007, ApJ, 658, 99
Myers, A. D., Richards, G. T., Brunner, R. J., et al. 2008, ApJ, 678, 635
Nesvadba, N. P. H., Lehnert, M. D., Eisenhauer, F., et al. 2006, ApJ, 650, 693
Oke, J. B., Cohen, J. G., Carr, M., et al. 1995, PASP, 107, 375
Osterbrock, D. E., & Ferland, G. J. (ed.) 2006, Astrophysics of Gaseous Nebulae
    and Active Galactic Nuclei (2nd ed.; Sausalito, CA: Univ. Science Books)
Peng, Z.-X., Chen, Y.-M., Gu, Q.-S., & Hu, C. 2011, Res. Astron. Astrophys.,
    11, 411
Piconcelli, E., Vignali, C., Bianchi, S., et al. 2010, ApJ, 722, L147
Probst, R. G., Gaughan, N., Abraham, M., et al. 2004, Proc. SPIE, 5492, 1716
Probst, R. G., George, J. R., Daly, P. N., Don, K., & Ellis, M. 2008, Proc. SPIE,
    7014, 70142S
Richstone, D., Ajhar, E. A., Bender, R., et al. 1998, Nature, 395, A14
Rodriguez, C., Taylor, G. B., Zavala, R. T., et al. 2006, ApJ, 646, 49
Rosario, D. J., McGurk, R. C., Max, C. E., et al. 2011, arXiv:1102.1733
Rosario, D. J., Shields, G. A., Taylor, G. B., Salviander, S., & Smith, K. L.
    2010, ApJ, 716, 131
Schlegel, D. J., Finkbeiner, D. P., & Davis, M. 1998, ApJ, 500, 525
Schmitt, H. R., & Kinney, A. L. 1996, ApJ, 463, 498
Schneider, D. P., Hall, P. B., Richards, G. T., et al. 2007, AJ, 134, 102
Shen, Y., Liu, X., Greene, J. E., & Strauss, M. A. 2011, ApJ, 735, 48
Shields, G. A., Bonning, E. W., & Salviander, S. 2009a, ApJ, 696, 1367
Shields, G. A., Rosario, D. J., Smith, K. L., et al. 2009b, ApJ, 707, 936
Smith, K. L., Shields, G. A., Bonning, E. W., et al. 2010, ApJ, 716, 866
Smith, K. L., Shields, G. A., Salviander, S., Stevens, A. C., & Rosario, D. J.
    2011, arXiv:1108.0383
Springel, V., Di Matteo, T., & Hernquist, L. 2005, MNRAS, 361, 776
Stern, D., Eisenhardt, P., Gorjian, V., et al. 2005, ApJ, 631, 163
Strateva, I. V., Strauss, M. A., Hao, L., et al. 2003, AJ, 126, 1720
Tadhunter, C. N., Fosbury, R. A. E., di Serego Alighieri, S., et al. 1988, MNRAS,
    235, 403
Tang, S., & Grindlay, J. 2009, ApJ, 704, 1189
van Dam, M. A., Le Mignant, D., & Macintosh, B. A. 2004, Appl. Opt., 43,
    5458
van Ojik, R., Roettgering, H. J. A., Carilli, C. L., et al. 1996, A&A, 313, 25
Villar-Martín, M., Alonso-Herrero, A., di Serego Alighieri, S., & Vernet, J.
    2000, A&AS, 147, 291
Villar-Martín, M., Sánchez, S. F., Humphrey, A., et al. 2007, MNRAS, 378, 416
Villar-Martín, M., Tadhunter, C., Pérez, E., et al. 2010, MNRAS, 407, L6
Vivek, M., Srianand, R., Noterdaeme, P., Mohan, V., & Kuriakosde, V. C. 2009,
    MNRAS, 400, L6
Wang, J., Chen, Y., Hu, C., et al. 2009, ApJ, 705, L76
Wang, J. X., Malhotra, S., Rhoads, J. E., et al. 2004, AJ, 127, 213
Xu, D., & Komossa, S. 2009, ApJ, 705, L20
Zhou, H., Wang, T., Zhang, X., Dong, X., & Li, C. 2004, ApJ, 604, L33
Zirm, A. W., Overzier, R. A., Miley, G. K., et al. 2005, ApJ, 630, 68